Electronic Supplementary Material (ESI) for RSC Advances.

Electronic Supplementary Information

Modelling Drug Adsorption in Metal-Organic Frameworks: The Role of Solvent

Abhishek T. Sose[1‡], Hannah D. Cornell[2‡], Bradley J. Gibbons[2], Ashley A. Burris[2], Amanda J. Morris[2*], and Sanket A. Deshmukh[1*]

[1]Department of Chemical Engineering, Virginia Tech, Blacksburg, VA, 24060, USA

[2]Department of Chemistry, Virginia Tech, Blacksburg, Virginia 24060, United States

‡ Both authors contributed equally

*Corresponding Authors: Dr. Sanket A. Deshmukh (sanketad@vt.edu), Dr. Amanda J. Morris (ajmorris@vt.edu)

Table of Contents:

Section S1. Simulation methods and atomic structures

The multi-purpose code RASPA[1] was used to perform Grand Canonical Monte Carlo (GCMC) simulations to investigate simulated drug adsorption in MOF. These simulations were performed at 300K similar to experimental room temperature conditions. **Table S1-3** and **Fig. S1** shows the structure of the atomistic model of 5-Fluorouracil, hydroxyurea and ethanol. These drugs were modeled as rigid. The ibuprofen model was modeled flexible using TraPPe force fields as used by Bernini et. al. to study adsorption of ibuprofen in selected MOFs.[2] Non-bonded interactions for drug-drug, ethanol-drug, ethanol-ethanol, ethanol-MOF and drug-MOF were described by Lennard-Jones (LJ) + coulomb potential. The parameters for the framework atoms and ethanol were taken from the Universal Force Field (UFF), while parameters for 5-fluorouracil and hydroxyurea were given by RASPA. Lorentz–Berthelot mixing rules were used for all cross-terms, and LJ interactions beyond 12 Å were neglected. Coulomb interactions were calculated using partial charges on the atoms, obtained by a charge equilibration method. The Ewald sum method was used to compute the electrostatic interactions. In this study, van der Waals interactions within a molecule are ignored since the molecule is modeled as rigid. Up to 1.5×10^6 Monte Carlo equilibration cycles and 0.5×10^6 production cycles for HKUST-1 and 0.5×10^6 equilibration cycles and 0.5×10^6 production cycles for NH_2-MIL-53 and UiOAZB were performed to calculate the ensemble averages.

Table S1. Ethanol rigid model coordinates

	x	y	z	epsilon	sigma	charge
C_1eth	-2.26008	-1.02342	-0.05466	52.836	3.431	-0.384129
C_2eth	-3.60131	-1.66677	-0.33496	52.836	3.431	0.175871
H_1eth	-1.8153	-0.64005	-0.97893	22.141	2.572	0.120607
H_2eth	-1.55828	-1.75727	0.35526	22.141	2.572	0.120625
H_3eth	-2.36347	-0.19866	0.65594	22.141	2.572	0.110374
O_1eth	-3.42077	-2.72825	-1.26034	30.192	3.119	-0.550437
H_4eth	-4.2965	-3.11954	-1.42011	22.141	2.572	0.355333
H_5eth	-4.29428	-0.93782	-0.76564	22.141	2.572	0.025897
H_6eth	-4.03302	-2.07121	0.58544	22.141	2.572	0.025859

Table S2. 5-Fluorouracil rigid model coordinates

	x	y	z	epsilon	sigma	charge
C_1fluor	-1.26266	0.729	0	30.7	3.6	-0.020636
C_2fluor	0	0	0	30.7	3.6	0.058065
N_1fluor	-1.26266	2.157	0	80	3.2	-0.392957
H_1fluor	-2.19796	0.189	0	8	2.2	0.143563

C_3fluor	0	2.871	0	50	3.7	0.722025
H_2fluor	-2.16332	2.677	0	8	2.2	0.319527
O_1fluor	0	4.221	0	100	2.96	-0.575592
N_2fluor	1.26266	2.157	0	80	3.2	-0.507838
C_4fluor	1.26266	0.729	0	50	3.7	0.525953
H_3fluor	2.16332	2.677	0	8	2.2	0.33976
O_2fluor	2.43179	0.054	0	100	2.96	-0.484002
F_1fluor	0	-1.4	0	36.4834	3.0932	-0.127868

Table S3. Hydroxyurea rigid model coordinates

	x	y	z	epsilon	sigma	charge
C_1hurea	-4.245	0.363	-0.102	50	3.7	0.728605
O_1hurea	-4.065	1.529	-0.43	100	2.96	-0.58299
N_1hurea	-5.467	-0.224	-0.131	80	3.2	-0.753827
H_1hurea	-6.219	0.42	-0.346	8	2.2	0.349517
H_2hurea	-5.673	-0.883	0.607	8	2.2	0.333538
N_2hurea	-3.244	-0.476	0.312	80	3.2	-0.305879
O_2hurea	-1.944	0.085	0.188	93	3.02	-0.395815
H_3hurea	-2.138	1.005	-0.1	0	0	0.359954
H_4hurea	-3.308	-1.439	0.002	8	2.2	0.266897

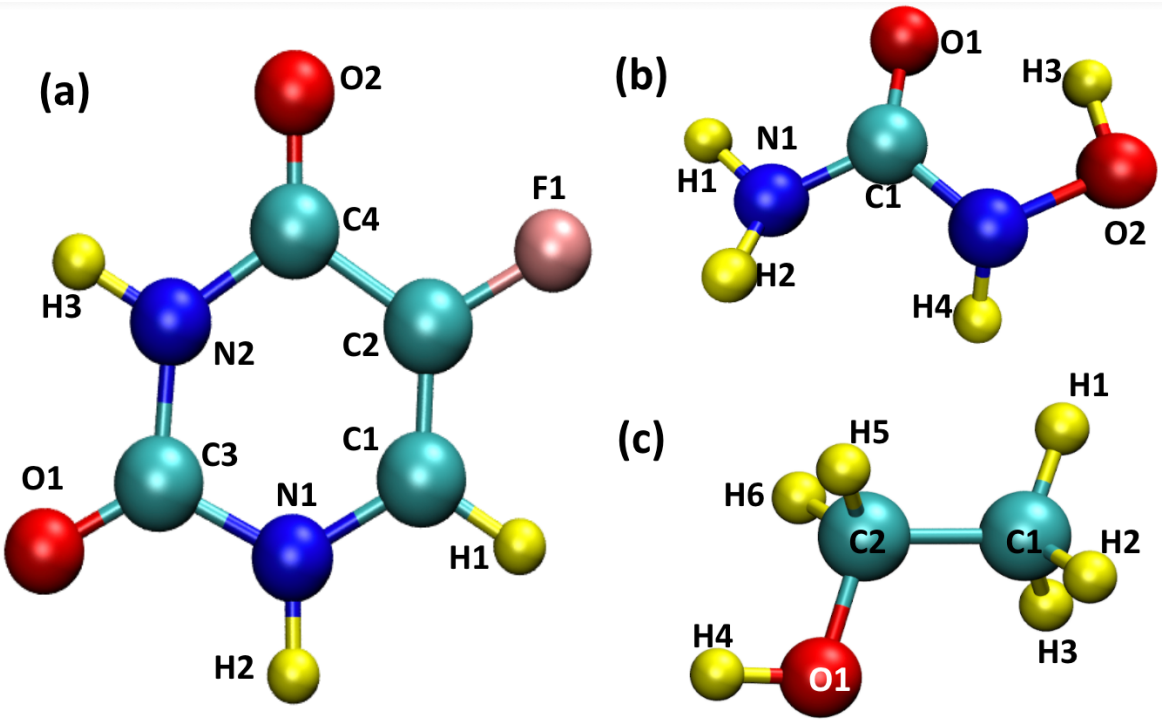

Figure S1. Model structures of (a) 5FU, (b) HU and (c) ethanol, with labels used for atoms for which RDF is calculated.

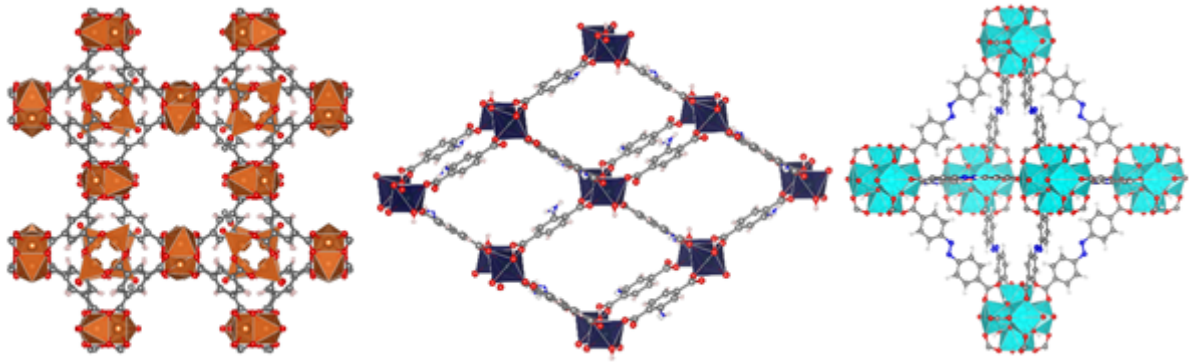

Figure S2. Crystal structures of HKUST-1, NH_2-MIL-53 and UiO-AZB (shown left to right)

Section S2: Synthesis and Characterization of MOFs

HKUST-1 and NH_2-MIL-53 were selected because of their established biocompatibility and wide-use throughout the literature.[3-8] UiO-AZB is a light-responsive framework developed in our lab that shows promise as a versatile drug delivery vehicle.[9,10]

Materials

The following chemicals were purchased from Sigma-Aldrich (St. Louis, MO, USA): copper nitrate hemipentahydrate (98%), 1,3,5-benzenetricarboxylic acid (trimesic acid, 98%), $ZrCl_4$ (≥99%), 5-fluorouracil (≥99%) and ibuprofen sodium salt (≥98%). Aluminum nitrate nonahydrate (≥99.8%) and 2-aminoterephthalic acid (98%) were purchased from TCI Chemicals. Hydroxyurea

was obtained from Oakwood Chemical (Estill, SC, USA). Ethanol, glacial acetic acid, and N,N-dimethylformamide (DMF, ≥99.8%) were obtained from Fisher Scientific (Hampton, NH, USA). Mitotane was purchased from Cayman Chemical Company. 4,4′-azobenzenedicarboxylic acid was synthesized as described in previous publications.[9,10]

Characterization Methods

Powder X-Ray Diffraction (PXRD). PXRD measurements were performed using a Rigaku Miniflex diffractometer (Cu Kα radiation λ= 1.5418 Å). Powder samples were loaded on a Rigaku Si510 sample holder disc and analyzed at a 0.05° resolution and a 5.0°/min continuous scanning mode over 2θ = 2−50°.

Thermogravimetric Analysis (TGA. Thermogravimetric Analysis was performed with a TGA 550 thermal analyzer (TA Instruments, New Castle, DE, USA). In a typical experiment, samples were heated at a ramp rate of 20 °C/min under nitrogen from 25–800 °C. All data was analyzed in TRIOS software (TA Instruments, New Castle, DE, USA) using the weight change function. A mass loss for drug cargo and MOF were obtained and used to calculate experimental drug loadings. The temperatures used for these calculations are included beneath each TGA plot.

N_2 Adsorption Isotherms (BET Surface Area Analysis). N_2 adsorption and desorption isotherms were collected using a Micrometrics 3-Flex surface analyzer (Micromeritics, Norcross, GA, USA). Prior to analysis, samples were placed in sample cells and activated under vacuum (0.1 mbar) for 24 h at temperatures appropriate for the frameworks (150 °C for HKUST-1, 120 °C UiO-AZB and 60 °C for NH_2-MIL-53). After analysis, PXRD was performed on each of the samples. PXRD data confirms that crystallinity was maintained throughout the activation/adsorption process.

MOF Synthesis

Synthesis of HKUST-1. HKUST-1 was synthesized via solvothermal synthesis using a literature procedure.[11] Copper nitrate hemipentahydrate (0.87 g) was placed in a vial and dissolved in 10 mL of water. In a second vial, 1,3,5-benzenetricarboxylic acid (0.47 g) was combined with 10 mL of ethanol. The vials were sonicated to fully dissolve the solids, then the aqueous solution was added to the second vial. The mixed solution was stirred for 10 min at room temperature. Next, 1 mL of DMF was added to the vial. The vial was sealed with Teflon tape, then heated at 85 °C for 20 h. After, the vial was cooled to room temperature. The resulting blue powder was collected via centrifugation, and washed once with ethanol and once with water. Next, the powder was washed vigorously with dichloromethane 5 times. Throughout the washing process, the powder become dark blue. After the final rinse, the powder was collected and dried in a vacuum oven overnight at 60 °C. The MOF powder was then stored in 120 °C oven until further use.

Synthesis of NH_2-MIL-53(Al). NH_2-MIL-53(Al) is synthesized through a common solvothermal synthesis.[12] In a vial, 2.5 mmol of 2-aminoterephthalic acid is dissolved in 8 mL of dimethylformamide (DMF). In a separate vial, 1.07 mmol of aluminum nitrate nonahydrate is dissolved in 8 mL of DMF. The vials are each sonicated until the solid is fully dissolved. At this point, the aluminum nitrate solution is added to the vial containing terephthalic acid. The combined solutions are sonicated briefly, then placed in an oven for 72 h at 120 °C. After 72 h, the off-white

powders are collected by centrifugation, washed 3 times with DMF, and 3 times with acetone. For further activation, the powder was collected and placed in a Teflon liner with DMF and heated to 150 °C in a Parr bomb for 72 h. After each day, fresh solvent was added to the liner. Next, the powders were collected via centrifugation and solvent exchanged in dichloromethane for an additional 72 h to remove residual DMF from the pores. Fresh solvent was added each day. The final powder was dried in a 60 °C vacuum oven.

Synthesis of UiO-AZB. UiO-AZB was synthesized as described in previous publications.[9,10] In a 6 dram vial, $ZrCl_4$ (0.0234 g, 0.1 mmol), glacial acetic acid (172 µL, 3 mmol), and DMF (5 mL) were combined and sonicated for ~5 min. Next, 4,4′-azobenzenedicarboxylic acid (0.0270 g, 0.1 mmol) was added to the vial and sonicated for an additional 5 min. The mixture was placed in a 120 °C oven for 24 h. The particles were collected via centrifugation, washed once with fresh DMF, and 5 times with ethanol. Upon removal of the final supernatant, the particles were dried in an oven at 60 °C for 3 days.

Drug Loading Procedure

For drug loading studies, drug solutions of 5-fluorouracil, ibuprofen, or hydroxyurea were prepared by dissolving 200 mg of drug in ethanol (10–30 mL). For hydroxyurea and 5-FU, additional heating to 60 °C for 0.5 h was needed to fully dissolve the drug. Next, 100 mg of MOF (HKUST-1, UiO-AZB, or NH_2-MIL-53) was added to the drug solution at room temperature. The solution was sonicated for 5–10 min, then stirred at room temperature for 72 h.* After this period, MOF powders were collected via centrifugation (~20 min). The samples were soaked in ethanol for 30 min and centrifuged down. The supernatant was decanted and the resulting powders were dried for 72 h in a 60 °C oven.

**For UiO-AZB + IBU and HKUST-1 + HU samples, frameworks degraded under extended lengths of stirring. Loading time was decreased to a 24 h period for these samples, which gave satisfactory PXRD patterns.*

MOF Characterization (prior to drug adsorption)

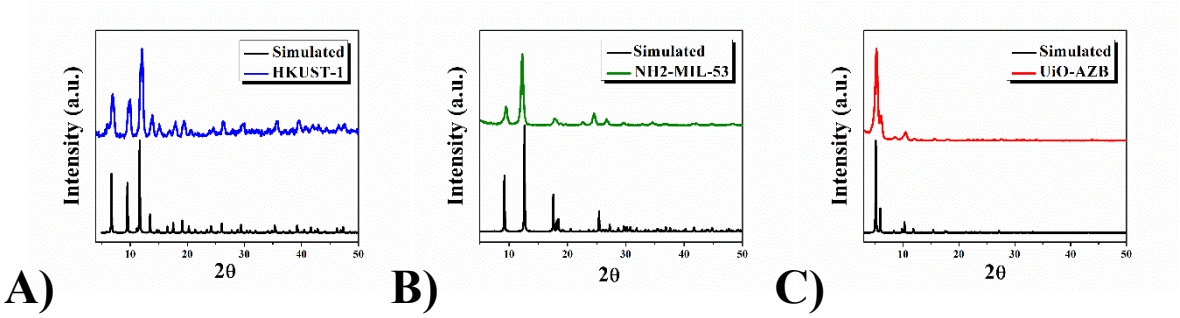

Figure S3. A) Experimental HKUST-1 powder pattern (blue) and simulated powder pattern obtained from available single crystal data[13] (black) **B)** Experimental NH_2-MIL-53 powder pattern (green) and simulated powder pattern obtained from available single crystal data[14] (black) **C)** Experimental UiO-AZB powder pattern (red) and simulated powder pattern obtained from available single crystal data[15] (black)

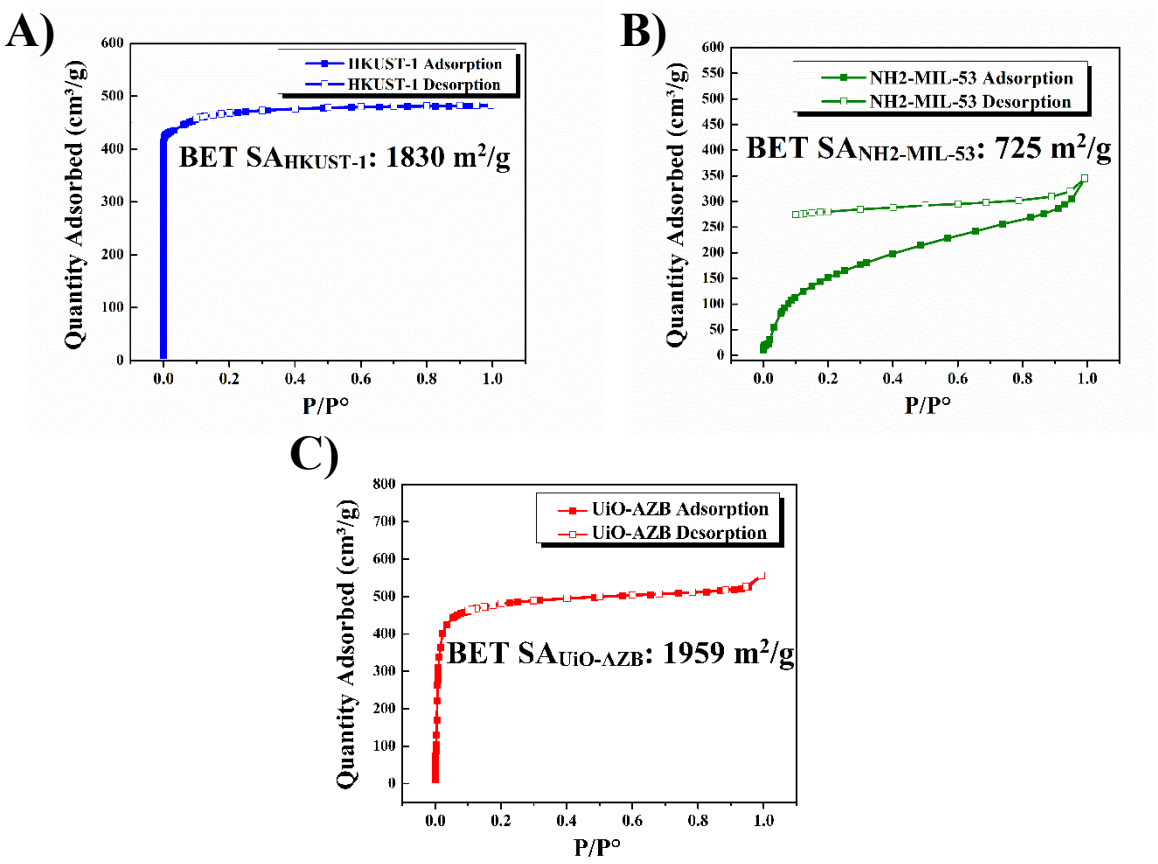

Figure S4. A) N_2 adsorption (blue solid square) and desorption (blue open square) isotherms for an unmodified HKUST-1 sample. The BET surface area was calculated to be 1830 m^2/g, which is consistent with previous values obtained for HKUST-1 synthesized by this procedure.[11] **B)** N_2 adsorption (green solid square) and desorption (green open square) isotherms for an unmodified NH_2-MIL-53 sample. The BET surface area was calculated to be 725 m^2/g, and is within error of other reported values (712 m^2/g)[16]. **C)** N_2 adsorption (red solid square) and desorption (red open square) isotherms for an unmodified UiO-AZB sample. The BET surface area was calculated to be 1959 m^2/g. This value is within error of values previously obtained for UiO-AZB MOF (~1900–2400 m^2/g).[17]

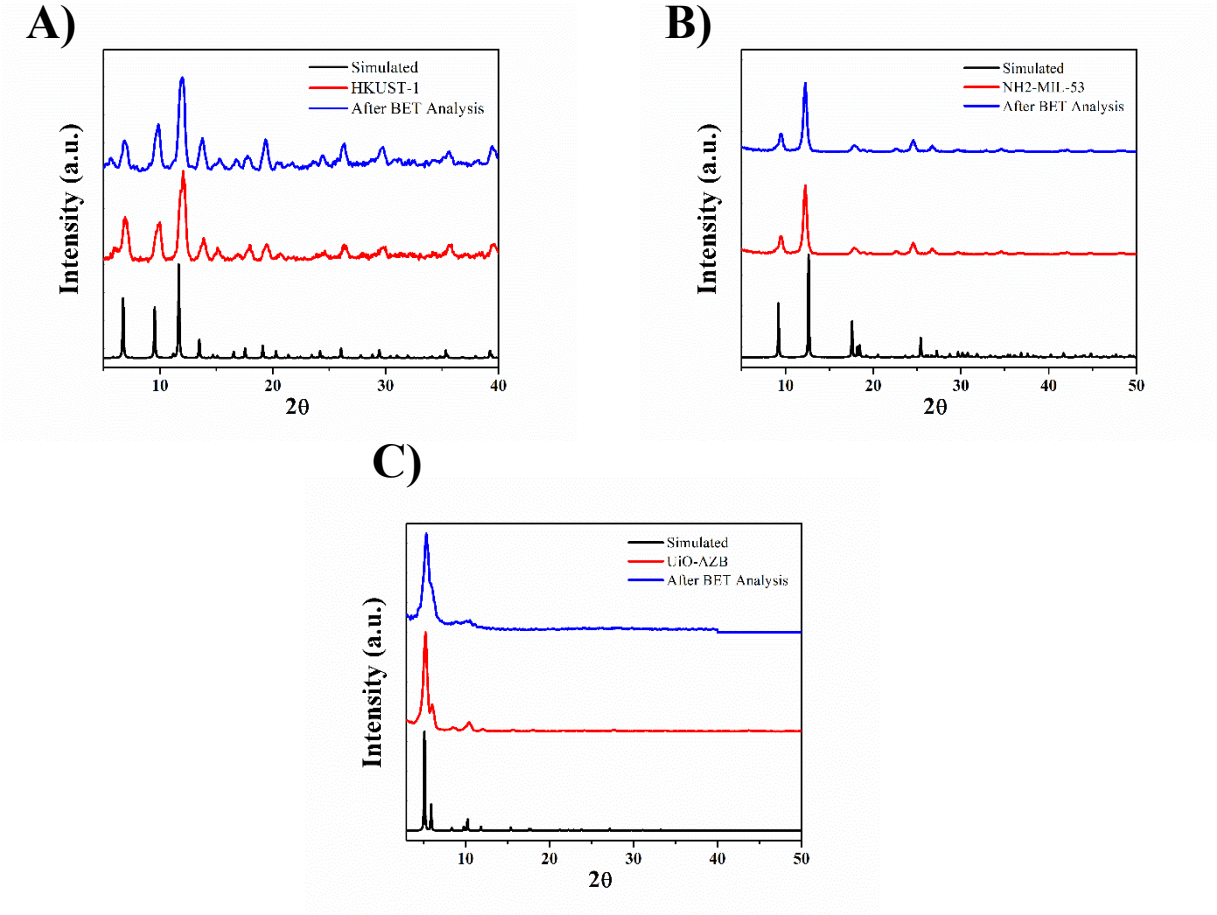

Figure S5. PXRD patterns for HKUST-1 (A), NH_2-MIL-53 (B), and UiO-AZB (C) after BET surface area measurements. The patterns remain unchanged, indicating crystallinity is maintained throughout the activation procedure.

MOF Characterization (after drug adsorption)

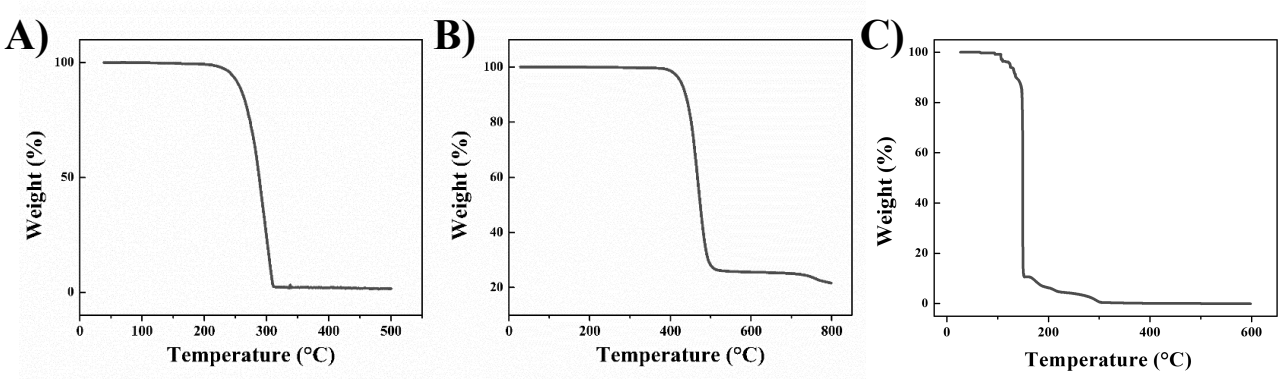

Figure S6. TGA weight loss profiles for 5-FU (A), IBU (B), and HU (C)

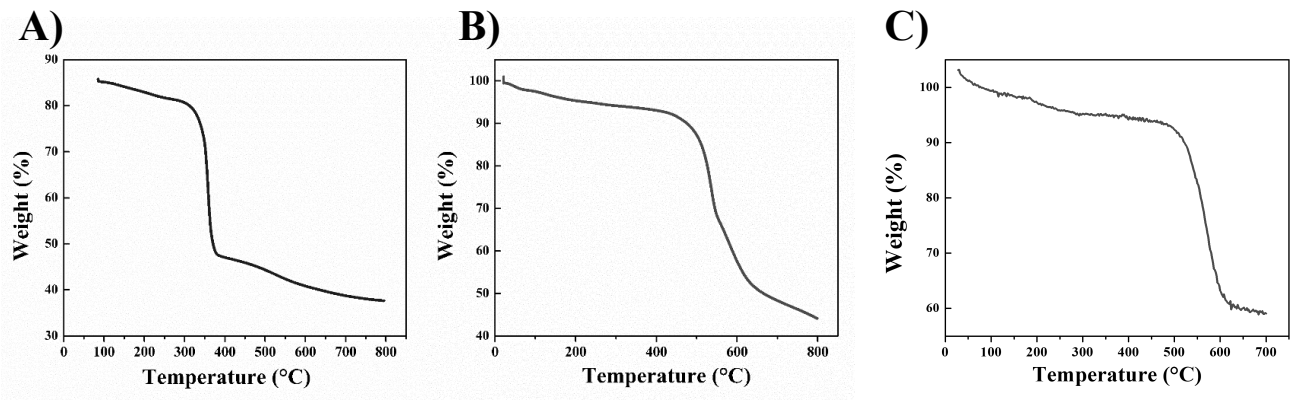

Figure S7. TGA weight loss profiles for HKUST-1 (A), NH2-MIL-53 (B), and UiO-AZB (C)

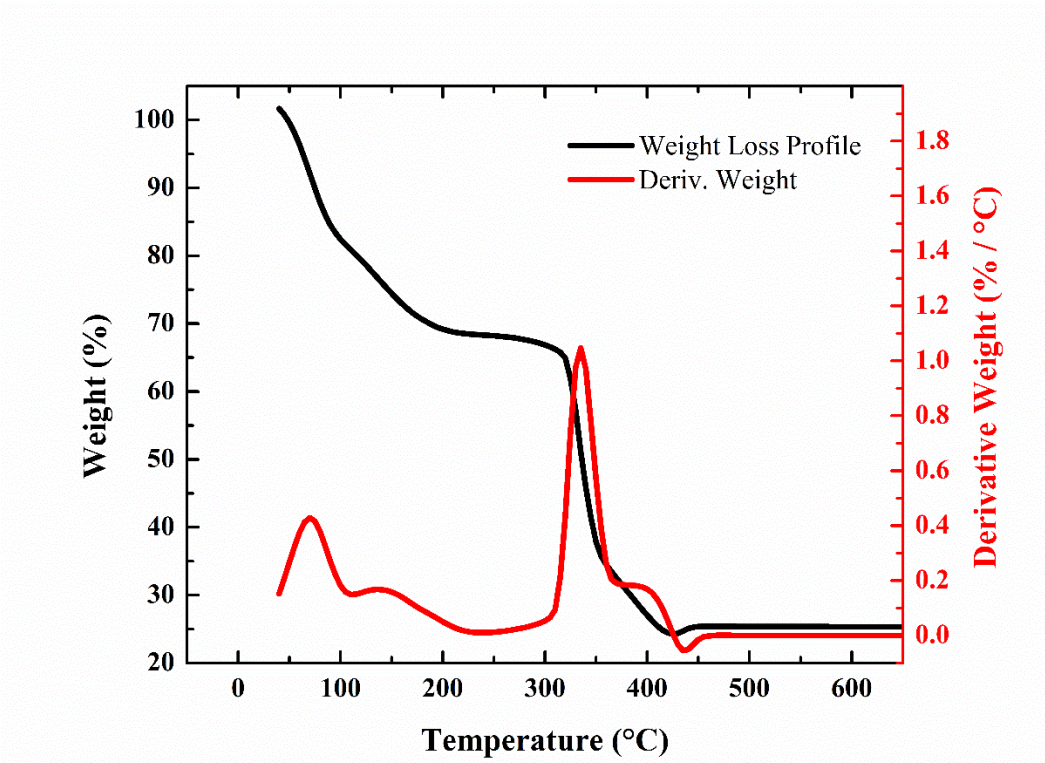

Figure S8. Weight loss profile (black) and derivative weight (red) as determined by TGA for HKUST-1 loaded with 5-FU. The profile shows three major weight losses: the first from 0 – 100 °C is attributed to loss of solvent (ethanol), the second (occurring between 150 – 250 °C) corresponds to loss of 5-FU, and the final loss (occurring between 300 – 450 °C) represents degradation of the framework. These drug loss ranges are consistent with other studies that measure loading of 5-FU in HKUST-1.[18]

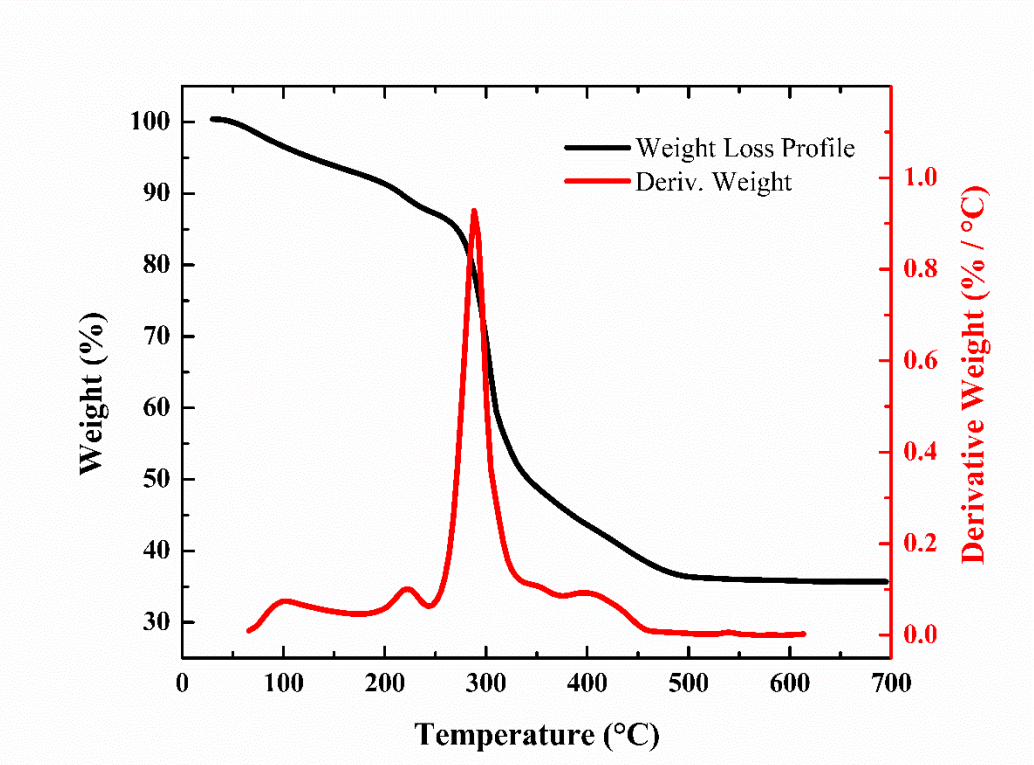

Figure S9. Weight loss profile (black) and derivative weight (red) as determined by TGA for HKUST-1 loaded with IBU. The profile shows three major weight losses: the first from 0 – 100 °C is attributed to loss of solvent (ethanol and water), the second (occurring between 175 – 275 °C) corresponds to loss of IBU, and the final loss (occurring between 275 – 450 °C) represents degradation of the framework. These drug loss ranges are consistent with other studies that measure loading of IBU in HKUST-1.[19]

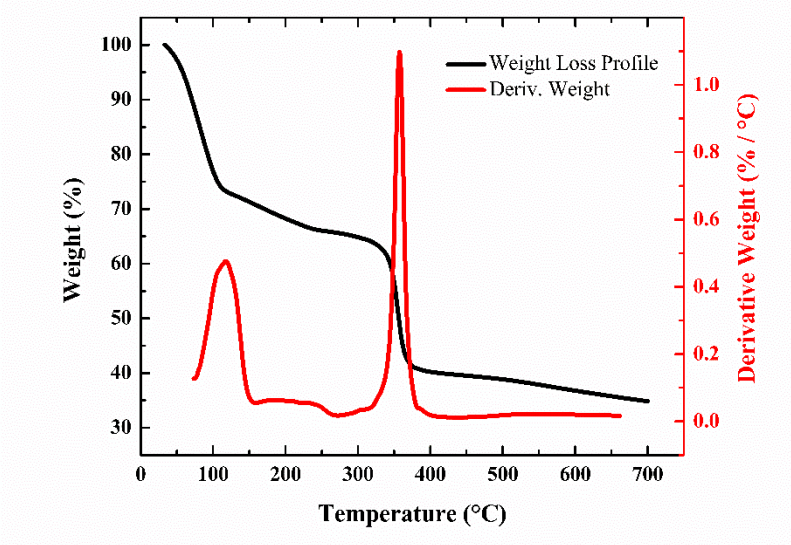

Figure S10. Weight loss profile (black) and derivative weight (red) as determined by TGA for HKUST-1 loaded with HU. The profile shows three major weight losses: the first from 0 – 100 °C is attributed to loss of solvent (ethanol and water), the second (occurring between 150 – 250 °C)

corresponds to loss of HU, and the final loss (occurring between 300 – 450 °C) represents degradation of the framework.

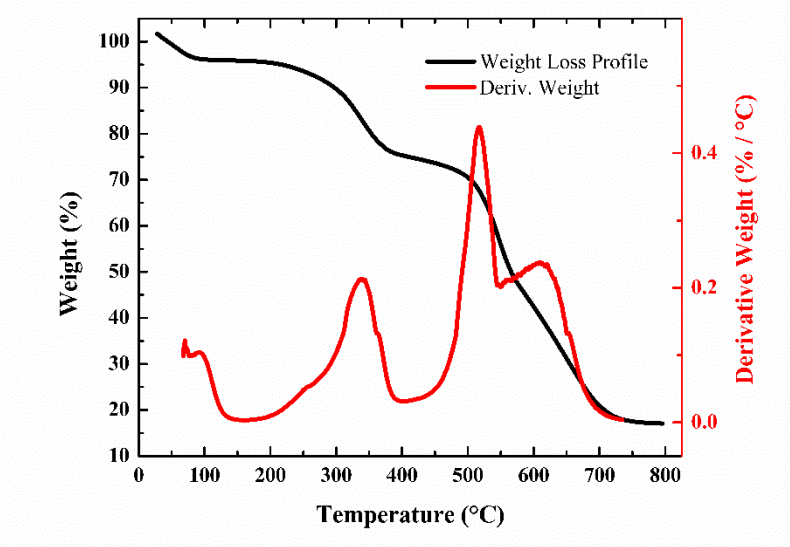

Figure S11. Weight loss profile (black) and derivative weight (red) as determined by TGA for NH_2-MIL-53 loaded with 5-FU. The profile shows three major weight losses: the first from 0 – 100 °C is attributed to loss of solvent (ethanol), the second (occurring between 150 – 400 °C) corresponds to loss of 5-FU, and the final loss (occurring between 450 – 650 °C) represents degradation of the framework.

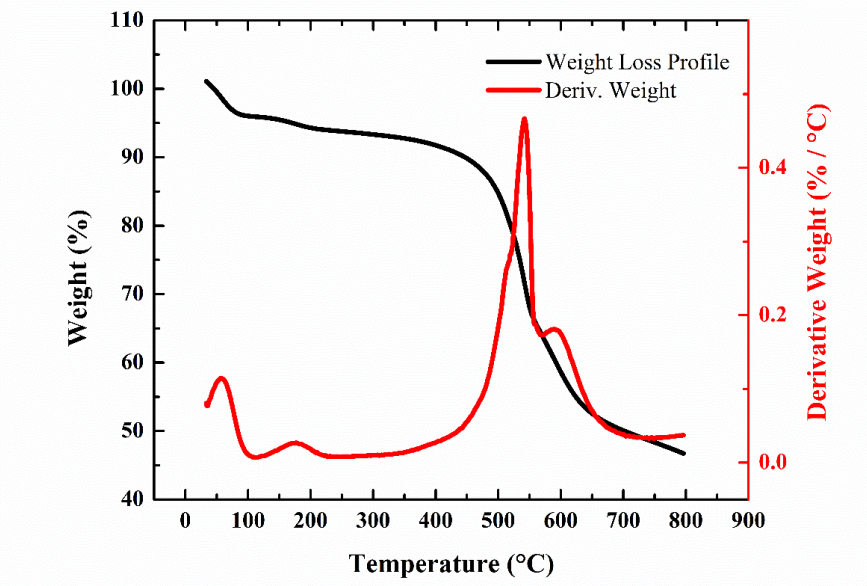

Figure S12. Weight loss profile (black) and derivative weight (red) as determined by TGA for NH_2-MIL-53 loaded with IBU. The profile shows three major weight losses: the first from 0 – 110 °C is attributed to loss of solvent (ethanol, water), the second (occurring between 110 – 250 °C) corresponds to loss of IBU[3], and the final loss (occurring between 400 – 750 °C) represents degradation of the framework.

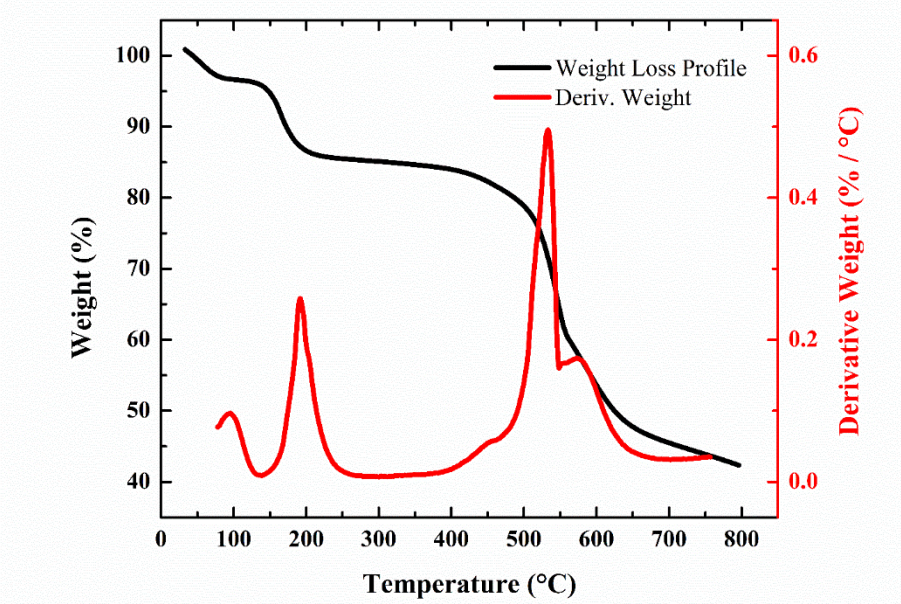

Figure S13. Weight loss profile (black) and derivative weight (red) as determined by TGA for NH_2-MIL-53 loaded with HU. The profile shows three major weight losses: the first from 0 – 140 °C is attributed to loss of solvent (ethanol), the second (occurring between 150 – 300 °C) corresponds to loss of HU, and the final loss (occurring between 400 – 675 °C) represents degradation of the framework.

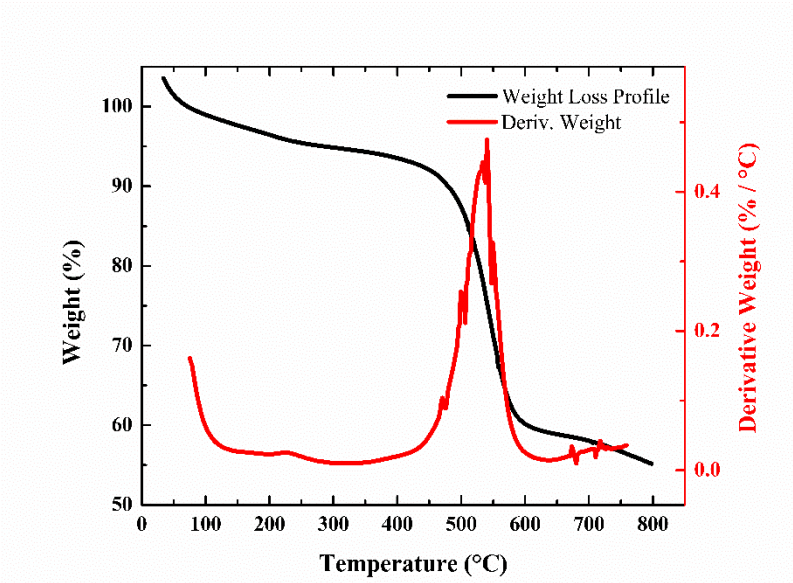

Figure S14. Weight loss profile (black) and derivative weight (red) as determined by TGA for UiO-AZB loaded with 5-FU. The profile shows three major weight losses: the first from 0 – 110 °C is attributed to loss of solvent (ethanol), the second (occurring between 150 – 300 °C) corresponds to loss of 5-FU, and the final loss (occurring between 450 – 600 °C) represents degradation of the framework.

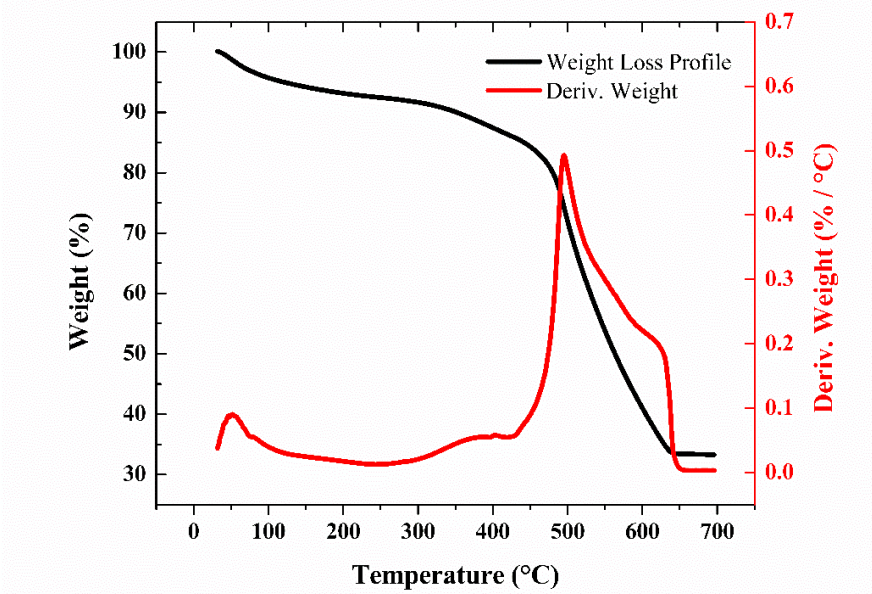

Figure S15. Weight loss profile (black) and derivative weight (red) as determined by TGA for UiO-AZB loaded with IBU. The profile shows three major weight losses: the first at 0 – 100 °C is attributed to loss of solvent (ethanol), the second from 200 – 400 °C corresponds to loss of IBU and the final loss occurring between 500 – 600 °C represents degradation of the framework.

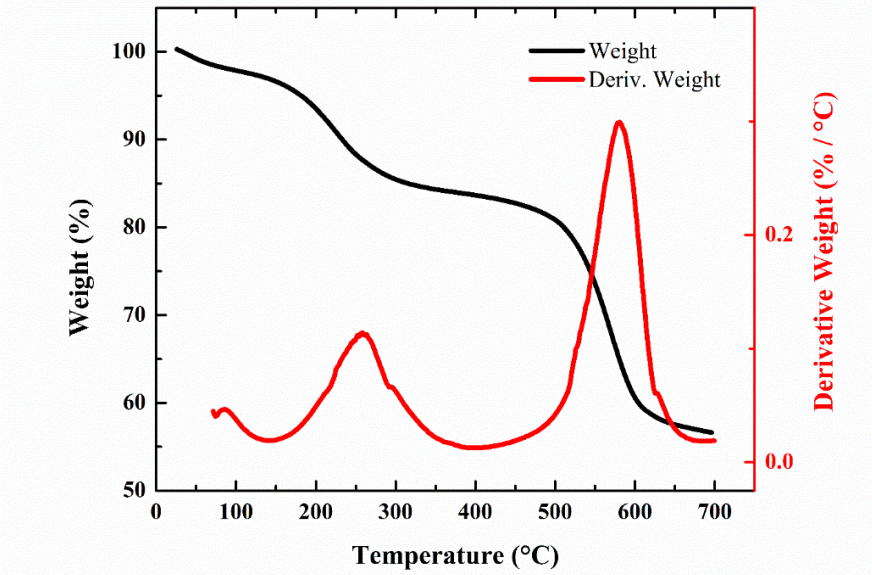

Figure S16. Weight loss profile (black) and derivative weight (red) as determined by TGA for UiO-AZB loaded with HU. The profile shows three major weight losses: the first from 0 – 120 °C is attributed to loss of solvent (ethanol), the second occurring between 150 – 400 °C corresponds to loss of HU, and the final loss occurring between 450 – 675 °C is due to degradation of the framework.

Table S4. Experimental drug adsorption values for HKUST-1, NH_2-MIL-53 and UiO-AZB

	5-FU loading (wt %)	IBU loading (wt %)	HU loading (wt %)
HKUST-1	15 ± 1	13 ± 2	30 ± 7
NH_2-MIL-53	19 ± 9	10 ± 1	44 ± 15
UiO-AZB	12 ± 2	18 ± 4	29 ± 2

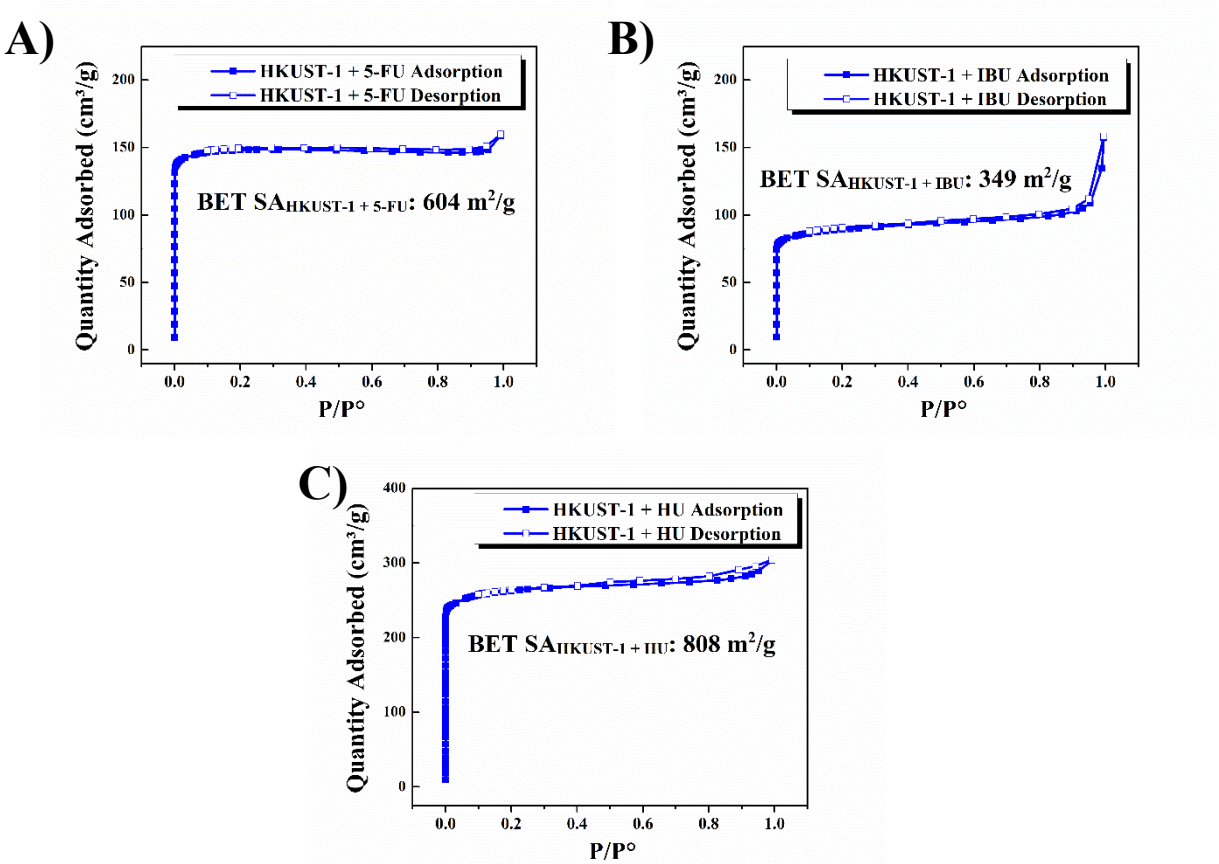

Figure S17. N_2 adsorption (blue solid square) and desorption (blue open square) isotherms for HKUST-1 samples loaded with 5-fluorouracil **(A)**, ibuprofen **(B)**, and hydroxyurea **(C)**. The BET surface areas were calculated to be 604, 349, and 808 m^2/g respectively.

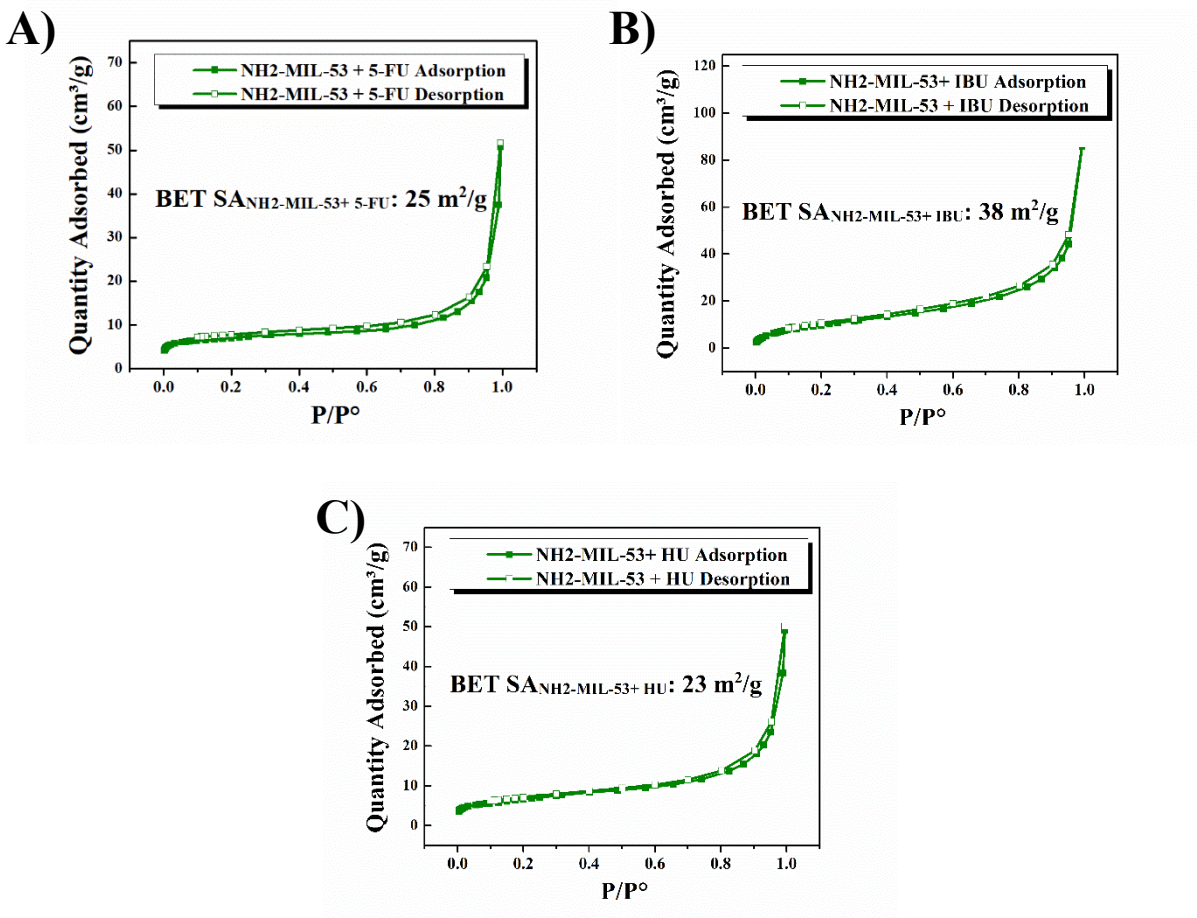

Figure S18. N_2 adsorption (blue solid square) and desorption (blue open square) isotherms for NH_2-MIL-53 samples loaded with 5-fluorouracil **(A)**, ibuprofen **(B)**, and hydroxyurea **(C)**. The BET surface areas were calculated to be 25, 38, and 23 m^2/g respectively. All NH_2-MIL-53 drug loaded samples show negligible residual porosity. These findings are consistent with other studies that show drug molecules block the one-dimensional pore of the framework, therefore limiting nitrogen adsorption sites.[20]

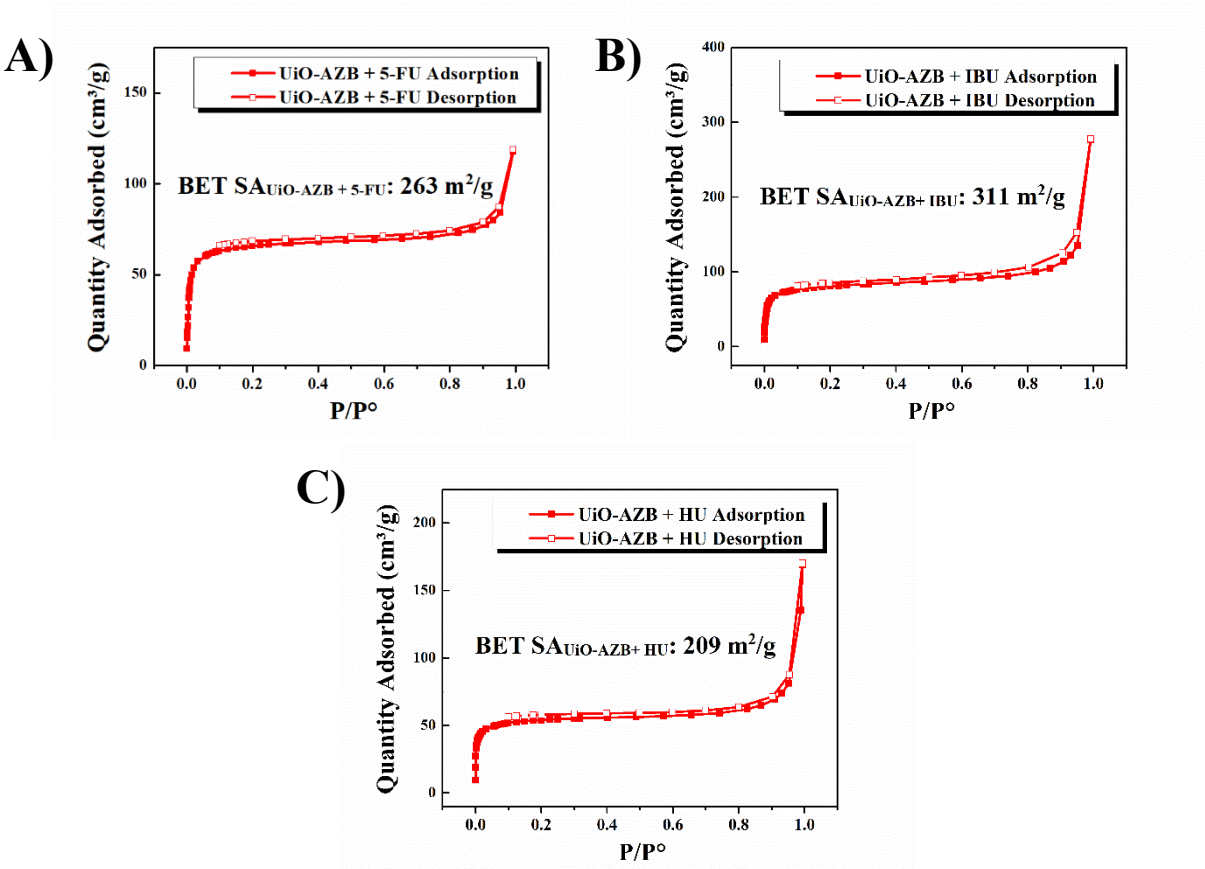

Figure S19. N_2 adsorption (red solid square) and desorption (red open square) isotherms for UiO-AZB samples loaded with 5-fluorouracil **(A)**, ibuprofen **(B)**, and hydroxyurea **(C)**. The BET surface areas were calculated to be 263, 311, and 209 m^2/g respectively. Overall, the drug loaded samples showed a 7-8 fold decrease in surface area as compared to UiO-AZB, which is consistent with findings of other drug loaded UiO type MOFs.[21]

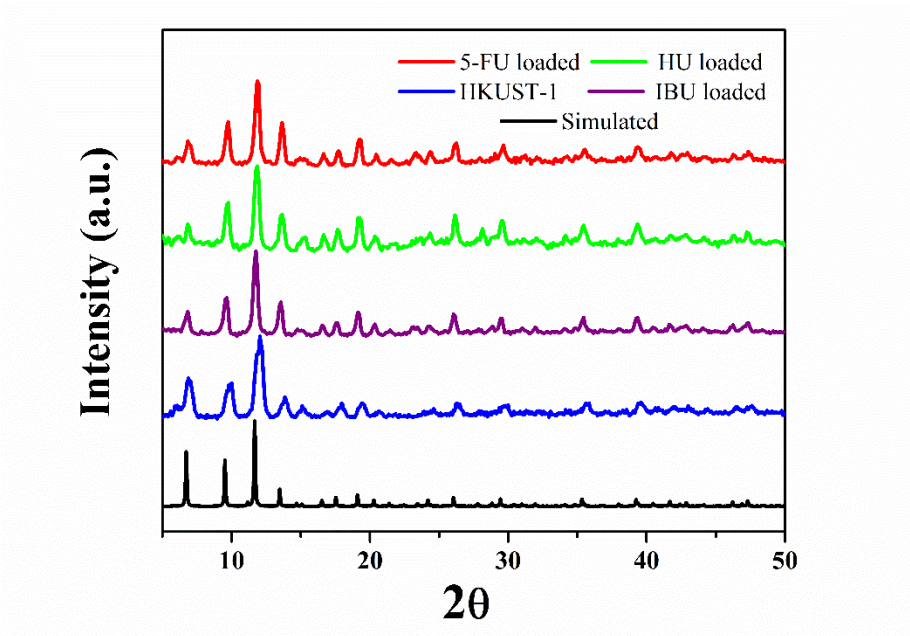

Figure S20. PXRD patterns for HKUST-1 samples. Unmodified MOF (blue) and HKUST-1 loaded with 5-FU (red), HU (green), and IBU (purple) are plotted alongside simulated patterns obtained from available single crystal data (black).

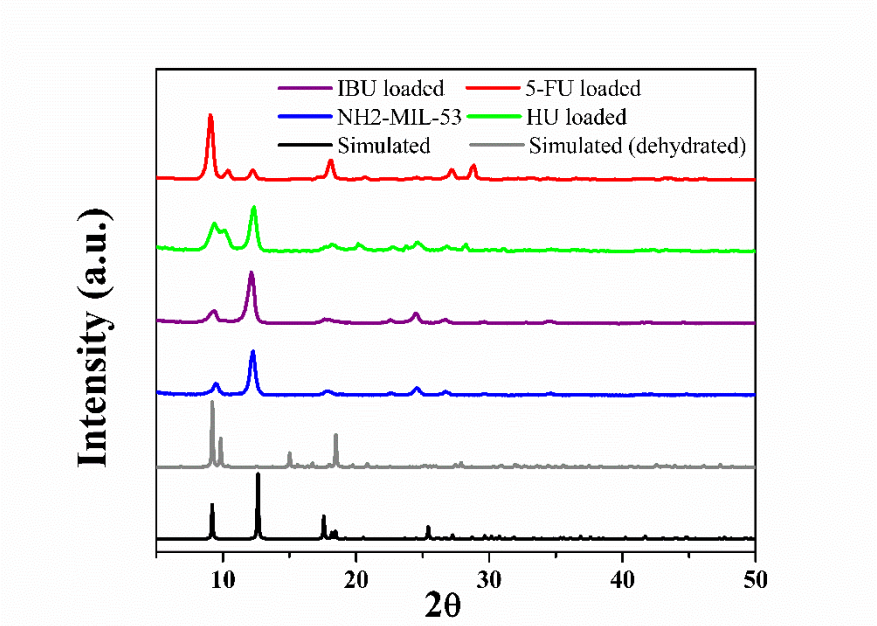

Figure S21. PXRD patterns for NH_2-MIL-53 samples. Unmodified MOF (blue) and NH_2-MIL-53 loaded with 5-FU (red), HU (green), and IBU (purple) are plotted alongside simulated patterns obtained from available single crystal data (black). The appearance of a peak at 10.5° in the 5-FU and HU samples is attributed to the presence of the dehydrated form of NH_2-MIL-53 (shown in grey).

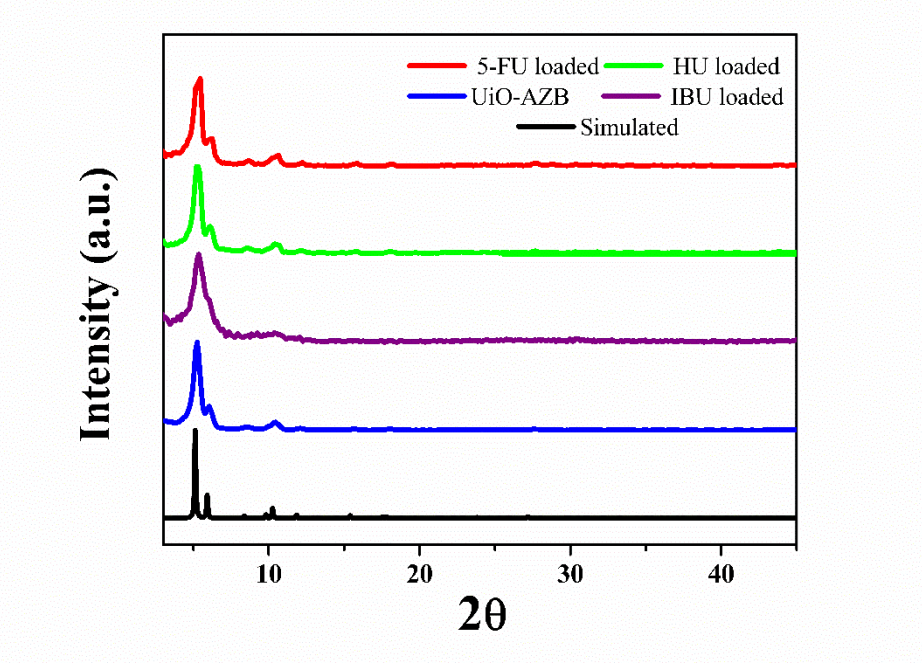

Figure S22. PXRD patterns for UiO-AZB samples. Unmodified MOF (blue) and UiO-AZB loaded with 5-FU (red), HU (green), and IBU (purple) are plotted alongside simulated patterns obtained from available single crystal data (black).

Section S3: Simulation methods in presence of ethanol

GCMC simulations were performed to study the adsorption of ethanol in the MOFs. Upto 1500000 equilibration cycles and 500000 production cycles were run to determine the maximum uptake capacity of ethanol in HKUST-1, while $0.5x10^6$ equilibration steps and $0.5x10^6$ production cycles were run for all drugs in NH_2MIL53 and $1.0x10^6$ equilibration steps and $0.5x10^6$ production cycles for UiOAZB. Monte Carlo moves with equal probability of translation, rotation, insertion, deletion, random reinsertion, and regrowth of an existing molecule on ethanol (component 1) and drug (component 2) were allowed. Table S4-6 describes the Lennard-Jones potential of the framework atoms. The structural crystallographic information files (.cif) for all three MOFs are attached along with the supporting information.

Table S5. Lennard-jones parameters for HKUST-1 framework

	epsilon	sigma
Cu_	2.5161	3.11369
O_	30.192	3.119
C_	52.836	3.431
H_	22.141	2.572

Table S6. Lennard-jones parameters for NH_2-MIL-53 framework

	epsilon	sigma
Al_	155.998	3.91105
O_	30.192	3.119
C_	52.836	3.431
H_	22.141	2.572
N_	80	3.2

Table S7. Lennard-jones parameters for UiO-AZB framework

	epsilon	sigma
Zr_	34.7221	2.78317
O_	30.192	3.119
C_	52.836	3.431
H_	22.141	2.572
N_	38.9492	3.26256

Section S4. Further insights on structural correlation of MOF and drugs

a. With oxygen and nitrogen of framework in presence of ethanol

Fig. S23 and Fig. S24 provides further insights of structural correlations of drug atoms with oxygen and nitrogen atoms of MOFs respectively. In the case of CuBTC, atom N2 of 5FU better correlates with CuBTC oxygen (1st peak at 3.16 Å) compared to O1 and F1 (1st peaks at 3.49 Å and 3.13 Å). This may be attributed to the potential hydrogen bond where atom N2 (donor) forms better correlation with oxygen of Cu-BTC. Similarly, for IBU, atoms OH_ib, O_ib and C_ib better interact with O (1st peaks at 3.04 Å, 3.18 Å and 3.80 Å respectively), where OH (donor) forms a probable H-bond with O. On the other hand, in the case of hydroxyurea, atom O2 has similar interactions with O **as compared to Cu** (1st peak at 3.11 Å), which are better compared to O1, N1 and N2 (1st peaks at 3.16 Å, 3.32 Å, and 3.88 Å).

In NH_2-MIL-53, O1, N2 and F1 atoms of 5-FU don't form a strong correlation with oxygen (1st peak at 4.83, 3.68 and 3.82 Å respectively), whereas they have a better relation with nitrogens (1st peak at 2.96, 3.68 and 4.26 Å for F1, O1 and N2) of -NH_2 group of NH_2-MIL-53. This may be attributed to the possible formation of hydrogen bonds with the -NH_2 group as donors. Likely H-bonds of carboxylic group of IBU, formed by OH_ib with O of MOF (1st peak at 3.79 Å) and O_ib with N of -NH_2 (1st peak at 2.84 Å) functional group associatively give superior adsorption effect. Specifically, in hydroxyurea two distinct possible H-bonds formed by N1 with O (1st peak at 3.40 Å) and O2 with N of -NH_2(1st peak at 3.59 Å) of MOF respectively have significant effect on

adsorption. From this analysis, we can conclude that atoms incapable of forming hydrogen bonds form better structural correlations with unsaturated metal sites of MOF.

In the case of UiOAZB, the first peaks of pairs O-O1, O-F1 and O-N2 appear at 4.33 Å, 4.67 Å and 5.80 Å, suggesting a strong structural correlation of O of UiOAZB with O1, compared to F1 and N2. Further, O1 and N forms a better correlation (1st peak at 3.35 Å) compared to N2-N (1st peak at 3.80 Å) and F1-N (1st peak at 4.02 Å). With IBU, O of UiOAZB doesn't form a plausible structural correlation, whereas O_ib, OH_ib and C_ib forms a better structural correlation with nitrogens with 1st peaks at 3.90 Å, 4.00 Å and 4.83 Å respectively. In the case of HU, N1 of the exposed -NH_2 group forms a better S.C. with the O of MOF (1st peak at 3.32 Å) compared to O1 (1st peak at 4.67 Å) and O2 (1st peak at 4.12 Å). Interestingly, O2, O1 and N1 all form strong structural correlation with nitrogen of UiOAZB, with 1st peaks at 3.73 Å, 3.76 Å and 4.07 Å respectively.

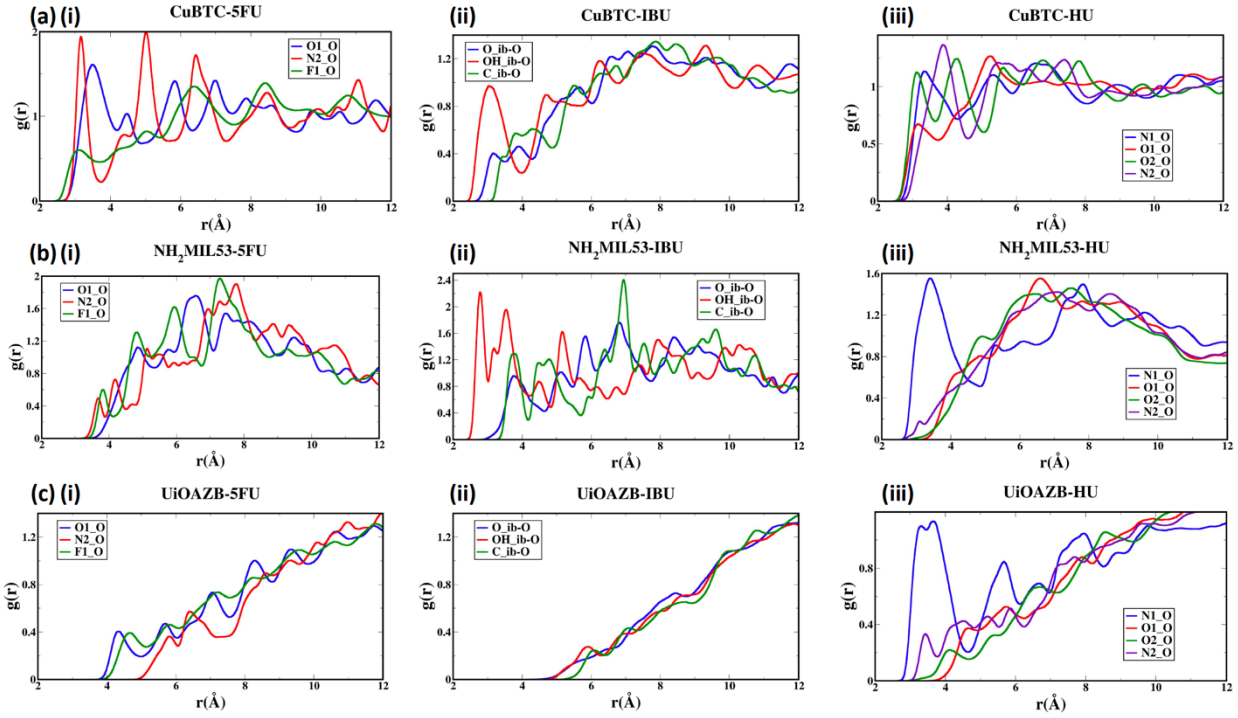

Figure S23. RDF of selected atoms of drugs with the oxygens of CuBTC, NH_2-MIL-53 and UiOAZB in the presence of ethanol

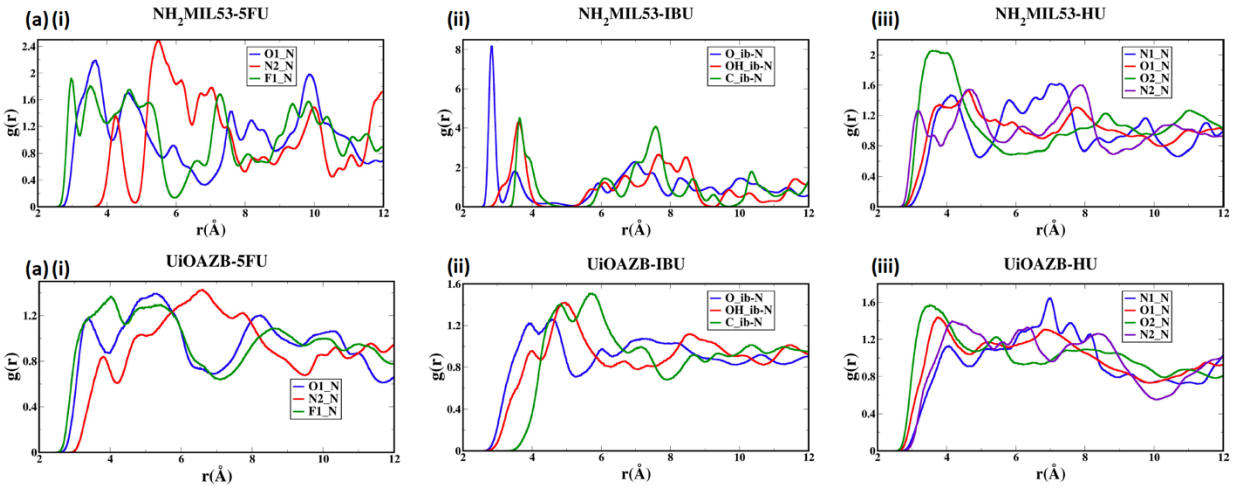

Figure S24. RDF of selected atoms of drugs with the nitrogens of NH_2-MIL-53 and UiOAZB in the presence of ethanol

b. With metals in absence of ethanol at 1 bar pressure

Fig. S25 (a), (b), and (c) show the RDF of metal atoms in CuBTC, NH_2-MIL-53 and UiO-AZB respectively, with atoms of 5FU, IBU and HU in the absence of ethanol. The first peaks for Cu-O1, Cu-N2, and Cu-F1 (Fig. S25 (a) i) pairs appear at 2.87 Å, 3.56 Å, and 3.11 Å, respectively. Similarly, peaks for IBU: Cu-OH_ib, Cu-O_ib and Cu-C_ib (1^{st} peaks at 3.11 Å, 3.52 Å and 3.54 Å respectively) and HU: Cu-N1, Cu-O1 and Cu-O2 (1^{st} peaks at 3.85 Å, 3.37 Å and 3.16 Å respectively) suggest a stronger correlation between Cu-OH_ib and Cu-O2 pairs, respectively. In the case of NH_2-MIL-53 a structural correlation between Al and O1 atoms (1^{st} peak at 4.50 Å) is stronger compared to between Al and N2 (1^{st} peak at 4.70 Å) and between Al and F1 (1^{st} peak at 6.28 Å) atoms of 5-FU (Fig. S25 (b) (i)). Interestingly, Al-O1 shows better correlation in absence of ethanol (1^{st} peak at 4.50 Å) compared to Al-N2 (1^{st} peak at 5.19 Å) in presence of ethanol. From the RDF of Al metal site of NH_2-MIL-53 with IBU and HU showing Al-OH_ib, Al-O_ib and Al-C_ib (1^{st} peaks at 4.00 Å, 7.07 Å and 7.02 Å respectively) and Al-N1, Al-O1 and Al-O2 (1^{st} peaks at 4.51 Å, 7.21 Å and 6.64 Å respectively) describe a stronger correlation with OH_ib and exposed -NH_2 group similar to what is evident in presence of ethanol. Similarly, for UiOAZB the Zr has stronger structural correlation with O1 (1^{st} peak at 5.99 Å) compared to F1 (1^{st} peak at 6.44 Å) and N2 (1^{st} peak at 5.46 Å) of 5-FU. In the case of carboxylic groups of IBU, OH_ib and C_ib shows a strong structural correlation with Zr metal sites unlike the RDFs in the presence of ethanol where no structural correlation was evident. This may be attributed to the presence of ethanol. Similar to the case in presence of ethanol, metal site (Zr) shows strongly ordered structure with the exposed -NH_2 group of HU with 1^{st} peak at 3.64 Å.

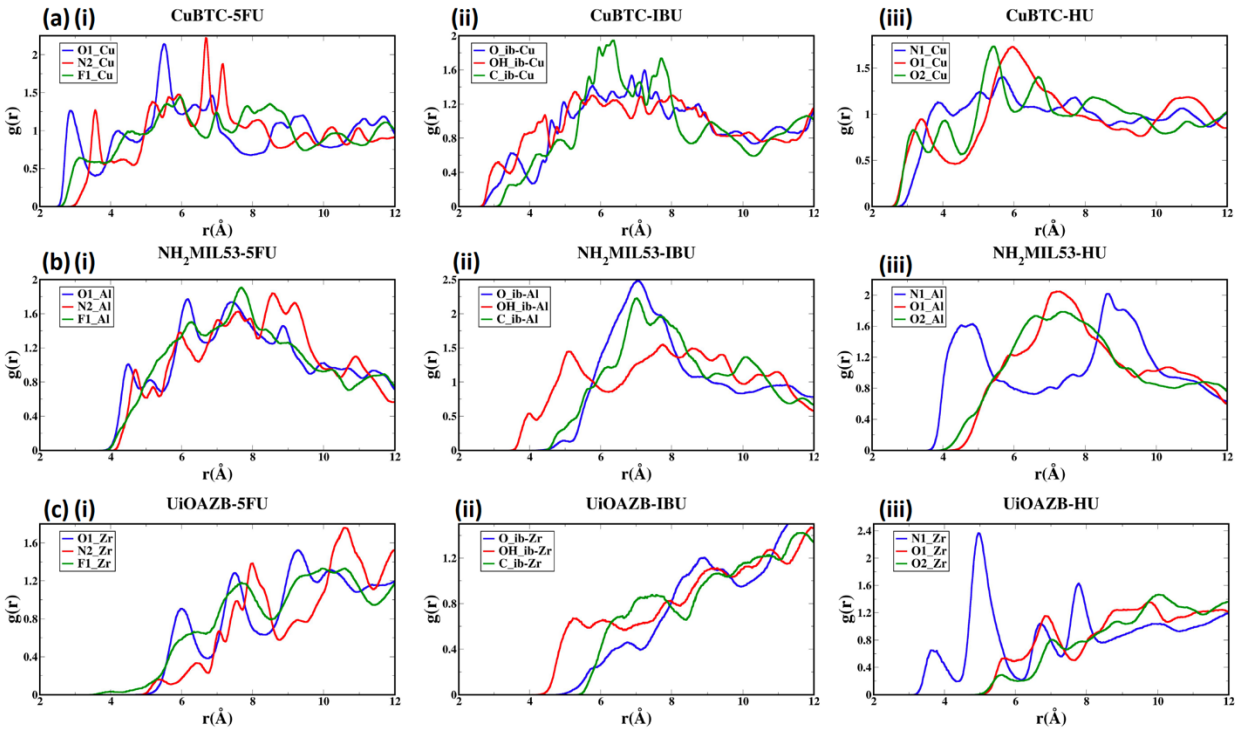

Figure S25. RDF of selected atoms of drugs with the unsaturated metal sites of CuBTC, NH_2-MIL-53 and UiOAZB **in the absence of ethanol** at 1 bar

Snapshots from GCMC simulations at low pressures suggested that the drug molecules were primarily adsorbed at the center of MOF pores. On the contrary, calculations at high pressure ($>10^{-5}$ bar) exhibited ethanol as the primary molecule adsorbed at the center of MOF pores. Furthermore, snapshots of NH_2-MIL-53 in presence of ethanol shows 5-FU molecules in ordered arrangement compared to in absence of ethanol. Moreover, in the case of UiOAZB, it is noticeable that the drug adsorption is similar, both in the presence and absence of ethanol. We further quantify the structural correlations of drugs with MOFs at lower pressure ranges by calculating RDF (Fig. S23 - 25). The peaks in the RDF show similar structure and strength of interactions between the drug and MOFs at lower pressures in the presence and absence of ethanol.

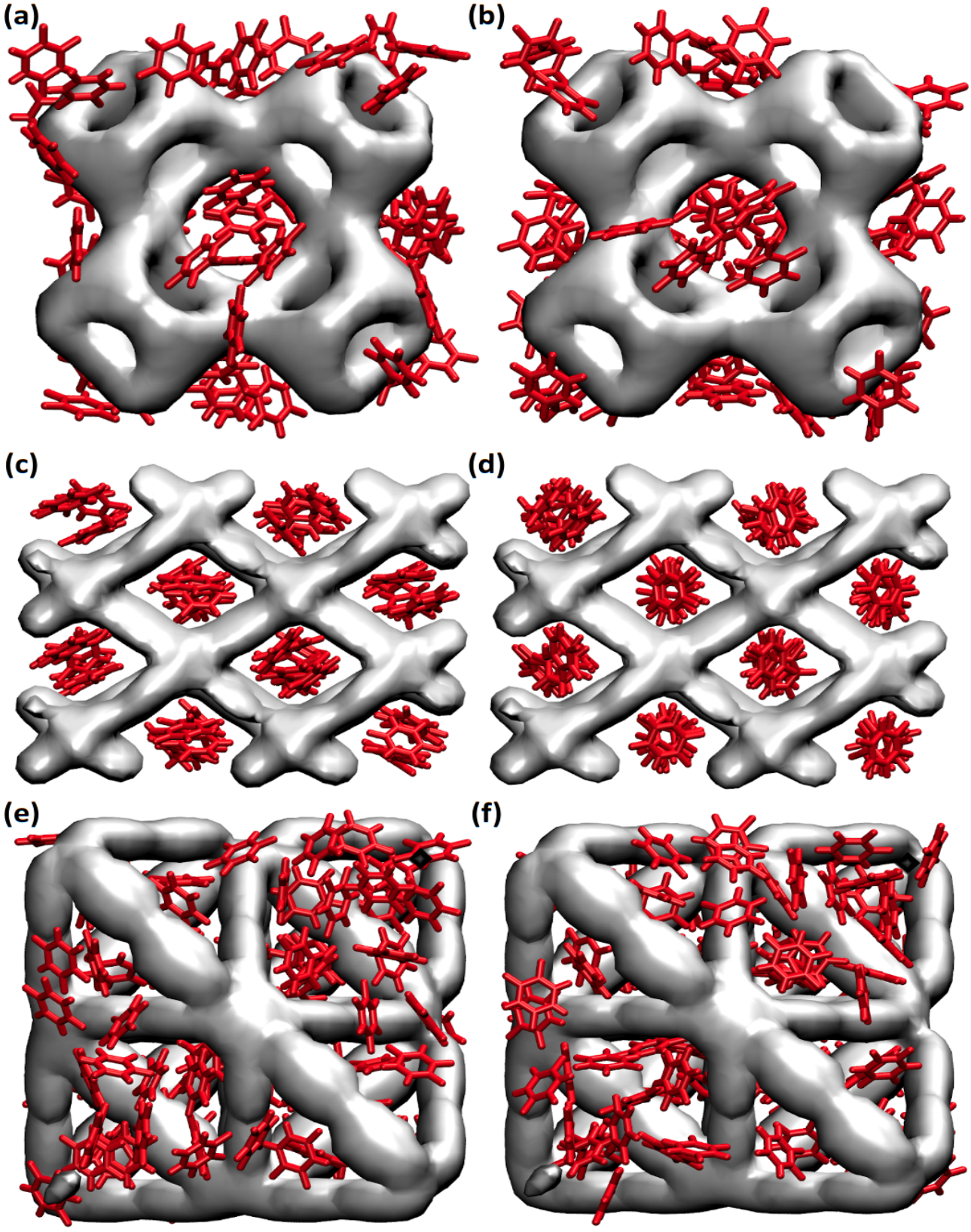
(a)
(b)
(c)
(d)
(e)
(f)

Figure S26: Snapshots of 5-FU in absence of ethanol in (a) CuBTC, (c) NH_2-MIL-53 and (e) UiO-AZB and in presence of ethanol (b), (d) and (f) respectively low-pressure range (10^{-4}, 10^{-12} and 10^{-4} Pa) in the presence and absence of ethanol. Ethanol molecules are not shown for clarity.

References:

1) Dubbeldam, D.; Calero, S.; Ellis, D. E.; Snurr, R. Q. RASPA: Molecular Simulation Software for Adsorption and Diffusion in Flexible Nanoporous Materials. *Mol. Simul.* **2016**, *42* (2), 81–101.
2) Bernini, M. C.; Fairen-Jimenez, D.; Pasinetti, M.; Ramirez-Pastor, A. J.; Snurr, R. Q. Screening of Bio-Compatible Metal–organic Frameworks as Potential Drug Carriers Using Monte Carlo Simulations. *J. Mater. Chem. B Mater. Biol. Med.* **2014**, *2* (7), 766–774.
3) Horcajada, P.; Serre, C.; Maurin, G.; Ramsahye, N. A.; Balas, F.; Vallet-Regí, M.; Sebban, M.; Taulelle, F.; Férey, G. Flexible Porous Metal-Organic Frameworks for a Controlled Drug Delivery. *J. Am. Chem. Soc.* **2008**, *130* (21), 6774–6780.
4) Leng, X.; Dong, X.; Wang, W.; Sai, N.; Yang, C.; You, L.; Huang, H.; Yin, X.; Ni, J. Biocompatible Fe-Based Micropore Metal-Organic Frameworks as Sustained-Release Anticancer Drug Carriers. *Mol. J. Synth. Chem. Nat. Prod. Chem.* **2018**, *23* (10).
5) Gao, X.; Zhai, M.; Guan, W.; Liu, J.; Liu, Z.; Damirin, A. Controllable Synthesis of a Smart Multifunctional Nanoscale Metal–Organic Framework for Magnetic Resonance/Optical Imaging and Targeted Drug Delivery. *ACS Appl. Mater. Interfaces* **2017**, *9* (4), 3455–3462.
6) Chen, Q.; Chen, Q.-W.; Zhuang, C.; Tang, P.-P.; Lin, N.; Wei, L.-Q. Controlled Release of Drug Molecules in Metal–Organic Framework Material HKUST-1. *Inorg. Chem. Commun.* **2017**, *79*, 78–81.
7) Latifi, L.; Sohrabnezhad, S. Drug Delivery by Micro and Meso Metal-Organic Frameworks. *Polyhedron* **2020**, *180*, 114321.
8) Li, Y.; Li, X.; Guan, Q.; Zhang, C.; Xu, T.; Dong, Y.; Bai, X.; Zhang, W. Strategy for Chemotherapeutic Delivery Using a Nanosized Porous Metal-Organic Framework with a Central Composite Design. *Int. J. Nanomedicine* **2017**, *12*, 1465–1474.
9) Epley, C. C.; Roth, K. L.; Lin, S.; Ahrenholtz, S. R.; Grove, T. Z.; Morris, A. J. Cargo Delivery on Demand from Photodegradable MOF Nano-Cages. *Dalton Trans. Camb. Engl. 2003* **2017**, *46* (15), 4917–4922.
10) Roth-Stefaniak, K.; Epley, C. C.; Novak, J. J.; McAndrew, M. L.; Cornell, H. D.; Zhu, J.; McDaniel, D. K.; Davis, J. L.; Allen, I. C.; Morris, A. J.; Grove, T. Z. Photo-Triggered Release of 5-Fluorouracil from a MOF Drug Delivery Vehicle. *Chem. Commun.* **2018**, *54* (55), 7617–7620.
11) Kim, H.K.; Yun, W.S.; Kim, M.; Kim, J.Y.; Bae, Y.; Lee, J.; Jeong, N.C. A Chemical Route to Activation of Open Metal Sites in the Copper-Based Metal–Organic Framework Materials HKUST-1 and Cu-MOF-2. **2015,** *J. Am. Chem. Soc. 137* (31), 10009–10015.
12) Cheng, X.; Zhang, A.; Hou, K.; Liu, M.; Wang, Y.; Song, C.; Zhang, G.; Guo, X. Size- and Morphology-Controlled NH2-MIL-53(Al) Prepared in DMF–Water Mixed Solvents. *Dalton Trans.* **2013**, *42* (37), 13698–13705.
13) Ahmed, A.; Hodgson, N.; Barrow, M.; Clowes, R.; Robertson, C. M.; Steiner, A.; McKeown, P.; Bradshaw, D.; Myers, P.; Zhang, H. Macroporous Metal–Organic Framework Microparticles with Improved Liquid Phase Separation. *J. Mater. Chem. A* **2014**, *2* (24), 9085–9090.

14) Alvarez, E.; Guillou, N.; Martineau, C.; Bueken, B.; Van de Voorde, B.; Le Guillouzer, C.; Fabry, P.; Nouar, F.; Taulelle, F.; de Vos, D.; et al. The Structure of the Aluminum Fumarate Metal–Organic Framework A520. *Angew. Chem. Int. Ed.* **2015**, *54* (12), 3664–3668.
15) Yang, Q.; Guillerm, V.; Ragon, F.; Wiersum, A. D.; Llewellyn, P. L.; Zhong, C.; Devic, T.; Serre, C.; Maurin, G. CH4 Storage and CO2 Capture in Highly Porous Zirconium Oxide Based Metal–Organic Frameworks. *Chem. Commun.* **2012**, *48* (79), 9831–9833.
16) Rostamnia, S.; Jafari, M. Metal–Organic Framework of Amine-MIL-53(Al) as Active and Reusable Liquid-Phase Reaction Inductor for Multicomponent Condensation of Ugi-Type Reactions. *Appl. Organomet. Chem.* **2017**, *31* (4), e3584.
17) Epley, C. C.; Love, M. D.; Morris, A. J. Characterizing Defects in a UiO-AZB Metal–Organic Framework. *Inorg. Chem.* **2017**, *56* (22), 13777–13784.
18) Souza, B. E.; Rudić, S.; Titov, K.; Babal, A. S.; Taylor, J. D.; Tan, J.-C. Guest–Host Interactions of Nanoconfined Anti-Cancer Drug in Metal–Organic Framework Exposed by Terahertz Dynamics. *Chem. Commun.* **2019**, *55* (27), 3868–3871.
19) Chen, Q.; Chen, Q.W.; Zhuang, C.; Tang, P.; Lin, N.; Wei, L.;. Controlled Release of Drug Molecules in Metal–Organic Framework Material HKUST-1. *Inorg. Chem. Commun.* **2017**, *79* , 78–81.
20) Pham, H.; Ramos, K.; Sua, A.; Acuna, J.; Slowinska, K.; Nguyen, T.; Bui, A.; Weber, M. D. R.; Tian, F. Tuning Crystal Structures of Iron-Based Metal–Organic Frameworks for Drug Delivery Applications. *ACS Omega* **2020**, *5* (7), 3418–3427.
21) Zhu, X.; Gu, J.; Wang, Y.; Li, B.; Li, Y.; Zhao, W.; Shi, J. Inherent Anchorages in UiO-66 Nanoparticles for Efficient Capture of Alendronate and Its Mediated Release. *Chem. Commun.* **2014**, *50* (63), 8779–8782.